

First-principles calculations of the superconducting properties in Li-decorated monolayer graphene within the anisotropic Migdal-Eliashberg formalism

Jing-Jing Zheng^{1,2} and E. R. Margine¹

¹*Department of Physics, Applied Physics and Astronomy, Binghamton University-SUNY, Binghamton, New York 13902, USA*

²*Institute of Theoretical Physics and Department of Physics, Shanxi University, Taiyuan 030006, People's Republic of China*

The *ab initio* anisotropic Migdal-Eliashberg formalism has been used to examine the pairing mechanism and the nature of the superconducting gap in the recently discovered lithium-decorated monolayer graphene superconductor. Our results provide evidence that the superconducting transition in Li-decorated monolayer graphene can be explained within a standard phonon-mediated mechanism. We predict a single anisotropic superconducting gap and a critical temperature $T_c = 5.1\text{-}7.6$ K, in very good agreement with the experimental results.

INTRODUCTION

During the past decade graphene has revolutionized many areas of nanotechnology from organic electronics to photovoltaics, plasmonics, photonics, and energy storage [1]. One notable application that was missing from this list was superconductivity, despite numerous theoretical predictions of either a conventional or an unconventional pairing mechanism [2–7]. Very recently, a high-resolution angle-resolved photoemission spectroscopy (ARPES) study has presented evidence supporting the appearance of a superconducting phase in Li-decorated monolayer graphene (LiC_6) around 5.9 K [8], within the standard phonon-mediated coupling mechanism. This work has been followed by two more studies that reported the observation of superconductivity in Ca-intercalated bilayer graphene [9] and in Ca-intercalated graphene laminates [10].

In this article, we investigate from first principles the nature of the superconducting gap in LiC_6 . To this end, we solve the fully anisotropic Migdal-Eliashberg equations [11, 12] to obtain the superconducting transition temperature (T_c) and the variation of the superconducting energy gap on the Fermi surface. While previous *ab initio* calculations have shown that the electron-phonon coupling is sufficient to yield a critical temperature in 6.7–10.3 K range using the Allen-Dynes formula [3, 13, 14] or the isotropic Eliashberg formalism [15], the nature of the superconducting gap has not yet been addressed. We find that, similar to bulk CaC_6 [15–18], Li-decorated monolayer graphene exhibits a single anisotropic gap in agreement with the experimental work [8].

METHODOLOGY

The calculations are performed within the local density approximation to density-functional theory [19, 20] using planewaves and norm-conserving pseudopotentials [21, 22], as implemented in the Quantum-ESPRESSO pack-

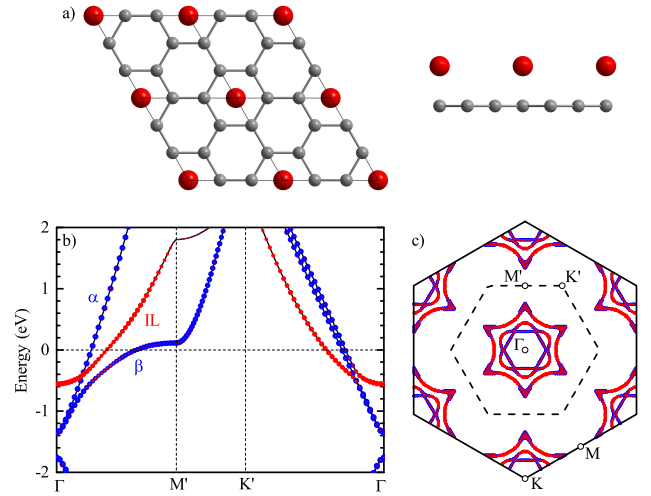


FIG. 1: (Color online)(a) Top- and side-view of a ball-and-stick model of LiC_6 , with C in gray and Li in red. (b) Band structure of LiC_6 . The inner and outer π^* bands (with respect to Γ point) are labeled as α and β (blue dots). The interlayer band is labeled as IL (red dots). The size of the blue and red symbols is proportional to the contribution of C- p_z and Li- s character. (c) The two-dimensional Fermi surface of LiC_6 with the same color code as in (b). The Brillouin zones of a graphene unit cell and a $\sqrt{3} \times \sqrt{3}R30^\circ$ graphene supercell are shown as black full and dashed lines, respectively.

age [23]. The planewaves kinetic energy cutoff is 100 Ry and the structural optimization is performed until the forces on atoms are less than $10 \text{ meV}/\text{\AA}$. Li-decorated monolayer graphene is described in the $\sqrt{3} \times \sqrt{3}R30^\circ$ graphene supercell with one lithium atom per unit cell. The optimized lattice constant and the adatom-graphene distance are $a = 4.24 \text{ \AA}$ and $h = 1.78 \text{ \AA}$. A Brillouin-zone (BZ) Γ -centered \mathbf{k} -point mesh of 24×24 and a Methfessel-Paxton smearing [24] of 0.02 Ry are adopted for the electronic charge density calculations. The phonon modes are computed within density-functional perturbation theory [25] on a 6×6 \mathbf{q} -mesh. We employ

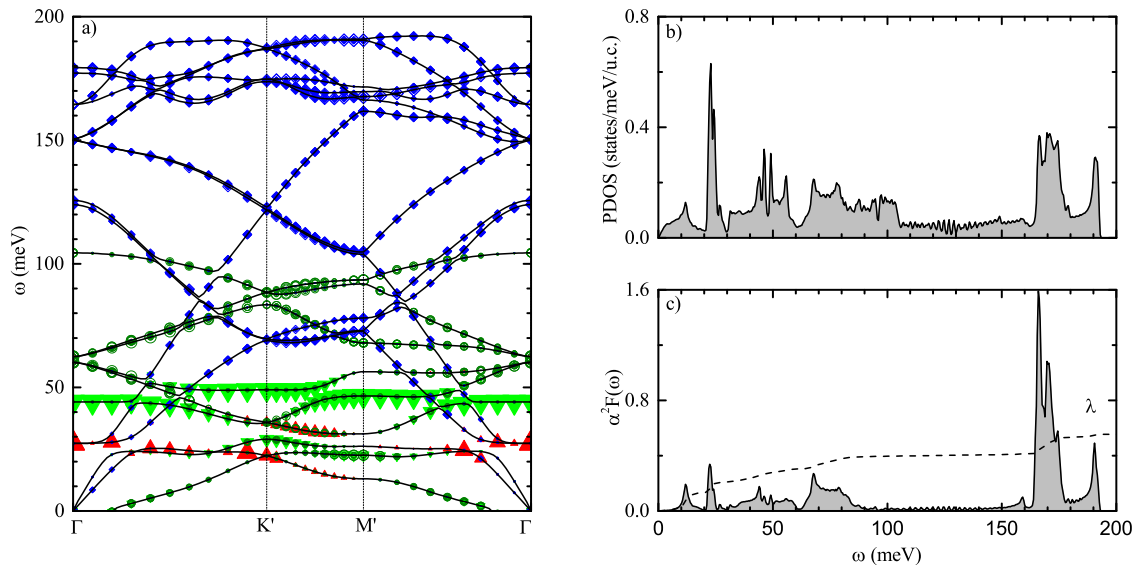


FIG. 2: (Color online) (a) Phonon frequency dispersion of LiC_6 . The decomposition of the phonon spectrum with respect to C and Li atomic vibrations is indicated by: olive circle (C_z), blue diamond (C_{xy}), red triangle up (Li_{xy}), and green triangle down (Li_z). (b) Phonon density of states and (c) Eliashberg spectral function with cumulative electron-phonon coupling strength of LiC_6 . The solid line is for $\alpha^2 F(\omega)$, the dashed line is for $\lambda(\omega)$.

the EPW code [12, 26–29] to obtain the superconducting gap. The calculation of the electronic wavefunctions required for the Wannier-Fourier interpolation [30, 31] in EPW is performed on a uniform unshifted BZ \mathbf{k} -point grid of size 12×12 . For the anisotropic Eliashberg equations, we use 120×120 and 60×60 \mathbf{k} - and \mathbf{q} -point grids. The Matsubara frequency cutoff is set to five times the largest phonon frequency (5×200 meV), and the Dirac delta functions are replaced by Lorentzians of widths 100 meV and 0.5 meV for electrons and phonons, respectively.

ELECTRONIC AND VIBRATIONAL PROPERTIES

In Figs. 1 (a)-(c), we show the crystal structure of Li-decorated monolayer graphene along with the corresponding decomposed electronic band structure and Fermi surface. Three bands cross the Fermi level around the Γ point, in agreement with previous reports [3, 13]. The inner and outer C π^* bands, labeled as α and β (blue dots), are obtained by folding the π^* states of graphene from K to Γ , following the superstructure induced by Li adsorption. The Li-derived band, labeled as IL (red dots), displays a nearly-free electron like dispersion upwards from about 0.56 eV below the Fermi energy. Similar weakly bound free-electron states have been observed in other layered materials [3, 32–34] and nanotubes [35], and their rapid downshift under doping is due to the combined effects of quantum confinement and electrostatic

response [3, 33, 35]. The corresponding Fermi surface of LiC_6 can be divided into two concentric regions centered around the Γ point. The inner region is characterized by a snowflake-like electron pocket intersecting a hexagonal electron pocket, which arises from the mixing of the inner C π^* states with the Li s states. These Fermi sheets resemble the Γ -centered Fermi surface observed in Ca and Li intercalated bilayer graphene [17, 36]. The outer region also has a snowflake-like shape and originates on the outer C π^* states and the Li s states.

We now focus on the vibrational properties and the electron-phonon coupling (EPC) in LiC_6 . Similar to bulk CaC_6 [32] and bilayer C_6CaC_6 [17], one can clearly identify in Fig. 2(a) three regions in the phonon dispersion associated to (i) the Li-related modes (up to 50 meV, where above 37 meV are Li_z modes mixed with carbon out-of-plane C_z modes), (ii) the carbon out-of-plane C_z vibrations (50-100 meV), and (iii) the carbon in-plane C_{xy} modes (above 100 meV). The size of the symbols in Fig. 2(a) is proportional to the atomic displacements corresponding to Li and C in-plane and out-of-plane contributions.

The isotropic Eliashberg spectral function $\alpha^2 F(\omega)$

$$\alpha^2 F(\omega) = \frac{1}{N_F N_{\mathbf{k}} N_{\mathbf{q}}} \sum_{\mathbf{k}, \mathbf{k}', \nu} |g_{\mathbf{k}\mathbf{k}'}^\nu|^2 \delta(\epsilon_{\mathbf{k}}) \delta(\epsilon_{\mathbf{k}'}) \delta(\omega - \omega_{\mathbf{q}\nu}), \quad (1)$$

and the cumulative electron-phonon coupling strength $\lambda(\omega)$

$$\lambda(\omega) = 2 \int_0^\omega d\omega' \alpha^2 F(\omega') / \omega', \quad (2)$$

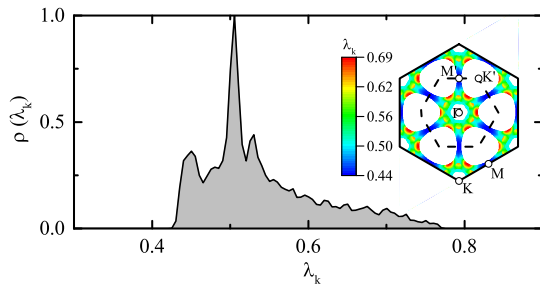


FIG. 3: (Color online) Distribution of the electron-phonon coupling strength $\lambda_{\mathbf{k}}$ of LiC_6 . Inset: Momentum-resolved electron-phonon coupling parameters $\lambda_{\mathbf{k}}$ on the Fermi surface (the data points correspond to electrons within ± 150 meV from the Fermi energy).

are shown in Figs. 2(b)-(c). In these expressions N_{F} represents the density of electronic states per spin at the Fermi level, $N_{\mathbf{k}}$ and $N_{\mathbf{q}}$ are the total numbers of \mathbf{k} and \mathbf{q} points, $\epsilon_{\mathbf{k}}$ is the Kohn-Sham eigenvalue with respect to the Fermi level, and $g'_{\mathbf{k}\mathbf{k}'}$ is the screened electron-phonon matrix element for the scattering between the electronic states \mathbf{k} and \mathbf{k}' through a phonon with wave vector $\mathbf{q} = \mathbf{k}' - \mathbf{k}$, frequency $\omega_{\mathbf{q}\nu}$ and branch index ν . Here \mathbf{k} and \mathbf{k}' indicate both the electron wavevector and the band index. We find that the low-energy phonons are key to achieving a high electron-phonon coupling in LiC_6 as they account for 0.28 (51%) of the total EPC ($\lambda = 0.55$). On the other hand, the electron-phonon coupling strengths associated with the out-of-plane C_z and in-plane C_{xy} modes are 0.12 (22%) and 0.15 (27%), respectively. Such behavior has also been found in bilayer C_6CaC_6 , where the most significant contribution to the EPC comes from the low-energy phonon modes [17]. Overall, our calculated EPC $\lambda = 0.55$ is in good agreement with the experimental value 0.58 ± 0.05 observed at the highest Li coverage [8] and the values reported in previous theoretical studies [3, 13].

To quantify the anisotropy in the electron-phonon coupling, we further evaluate the momentum-resolved EPC $\lambda_{\mathbf{k}}$ [12], defined as:

$$\lambda_{\mathbf{k}} = \sum_{\mathbf{k}', \nu} \delta(\epsilon_{\mathbf{k}'}) |g'_{\mathbf{k}\mathbf{k}'}|^2 / \omega_{\mathbf{q}\nu}. \quad (3)$$

The calculated $\lambda_{\mathbf{k}}$ displays a significant anisotropy with a distribution in the 0.42-0.78 range as shown in Fig. 3. This is in line with experimental ARPES measurements where a marked anisotropy in the electron-phonon coupling has been observed in the case of decorated graphene [8, 37], intercalated bilayer graphene [38], and intercalated graphite [39, 40]. An alternative way to look at the EPC anisotropy is presented in the inset of Fig. 3, where the variation of $\lambda_{\mathbf{k}}$ on the Fermi surface is shown. When compared with the Fermi surface plot in Fig. 1(c), one can clearly see that the largest value of $\lambda_{\mathbf{k}}$ is attained

on the portions of the Fermi surface dominated by the Li states. Notably, in bulk CaC_6 , $\lambda_{\mathbf{k}}$ was also found to be larger for the states with Ca dominant orbital character on the Fermi surface [16]. An important implication of this finding is that the IL state and its associated interaction play a critical role in the superconducting pairing of LiC_6 . A recent ARPES study has provided compelling evidence regarding the importance of the IL band in the pairing mechanism of bulk CaC_6 [41]. Furthermore, the lack of any sign of superconductivity down to 3.5 K in few-layer graphene under large charge doping induced by electrochemical gating [42] provides additional proof of the vital role of dopant atoms.

SUPERCONDUCTING PROPERTIES

The superconducting properties of LiC_6 are obtained by solving self-consistently the fully anisotropic Migdal-Eliashberg equations along the imaginary axis at the fermion Matsubara frequencies $\omega_n = (2n+1)\pi T$ (with n an integer) for each temperature T [4, 11, 12, 43]:

$$Z(\mathbf{k}, i\omega_n) = 1 + \frac{\pi T}{N_{\text{F}} \omega_n} \sum_{\mathbf{k}' n'} \frac{\omega_{n'}}{\sqrt{\omega_{n'}^2 + \Delta^2(\mathbf{k}', i\omega_{n'})}} \times \delta(\epsilon_{\mathbf{k}'}) \lambda(\mathbf{k}, \mathbf{k}', n - n'), \quad (4)$$

$$Z(\mathbf{k}, i\omega_n) \Delta(\mathbf{k}, i\omega_n) = \frac{\pi T}{N_{\text{F}}} \sum_{\mathbf{k}' n'} \frac{\Delta(\mathbf{k}', i\omega_{n'})}{\sqrt{\omega_{n'}^2 + \Delta^2(\mathbf{k}', i\omega_{n'})}} \times \delta(\epsilon_{\mathbf{k}'}) [\lambda(\mathbf{k}, \mathbf{k}', n - n') - \mu_c^*]. \quad (5)$$

$Z(\mathbf{k}, i\omega_n)$ is the mass renormalization function, $\Delta(\mathbf{k}, i\omega_n)$ is the superconducting gap function, $\lambda(\mathbf{k}, \mathbf{k}', n - n')$ is the momentum- and energy-dependent EPC, and μ_c^* is the semiempirical Coulomb parameter. The anisotropic $\lambda(\mathbf{k}, \mathbf{k}', n - n')$ to be used in the Eliashberg equations is given by:

$$\lambda(\mathbf{k}, \mathbf{k}', n - n') = N_{\text{F}} \sum_{\nu} \frac{2\omega_{\mathbf{q}\nu}}{(\omega_n - \omega_{n'})^2 + \omega_{\mathbf{q}\nu}^2} |g'_{\mathbf{k}\mathbf{k}'}|^2. \quad (6)$$

Figure 4(a) shows the superconducting energy gap $\Delta_{\mathbf{k}}$ as a function of temperature, calculated for a screened Coulomb parameter $\mu^* = 0.14$, together with the average value of the gap (red squares). The superconducting gap $\Delta_{\mathbf{k}}$ on different parts of the Fermi surface at 0.5 K is shown in Fig. 4(b). We find that monolayer LiC_6 displays a single anisotropic gap with an average value $\Delta_0 = 0.89$ meV in the $T = 0$ K limit, in very good agreement with the ARPES result of 0.9 ± 0.2 meV, measured at 3.5 K [8]. This situation is similar to bulk CaC_6 where the multiple-sheet Fermi surface gives rise to a single gap structure with a sizable anisotropy [16, 17], but unlike bilayer C_6CaC_6 for which a two gap structure has been recently predicted [17].

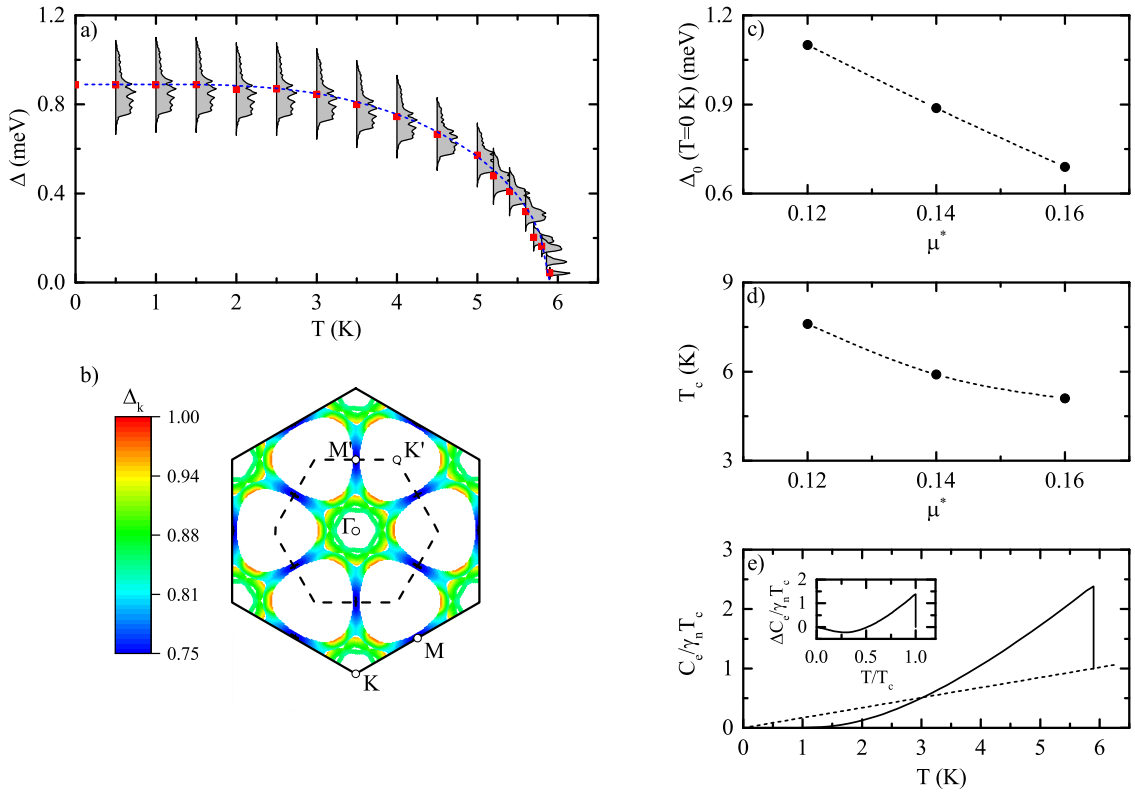


FIG. 4: (Color online) (a) Energy distribution of the anisotropic superconducting gap $\Delta_{\mathbf{k}}$ of LiC_6 as a function of temperature. The gap was calculated using a Coulomb pseudopotential μ^* of 0.14. The red squares represent the average value of the gap which vanishes at the critical temperature $T_c = 5.9$ K. The blue dashed line is the BCS fit to the calculated data. (b) Momentum-resolved superconducting gap $\Delta_{\mathbf{k}}$ (in meV) on the Fermi surface at 0.5 K. The data points correspond to electrons within ± 150 meV from the Fermi energy. (c) Calculated superconducting gap at the Fermi level in the $T = 0$ K limit as a function of the Coulomb parameter μ^* . (d) Calculated superconducting critical temperature as a function of the Coulomb parameter μ^* . (e) Normalized specific heat as a function of temperature for $\alpha = 1.75$ in the superconducting state (solid line) and normal state (dashed line). The specific heat difference between the normal and superconducting state versus reduced temperature is shown in the inset.

The superconducting T_c is identified as the highest temperature at which the gap vanishes. From Fig. 4(a) we find $T_c = 5.9$ K and a ratio $2\Delta_0/k_B T_c = 3.50$, very close to the ideal BCS value of 3.53 [44]. The predicted superconducting critical temperature is in excellent agreement with the experimental estimation of 5.9 K based on measurements of the size of the superconducting gap [8]. The temperature dependence of the superconducting gap can be well fitted with a BCS model, as obtained by solving numerically the BCS gap equation [45] with Δ_0 and T_c from our first-principles calculations. This is shown by the blue dashed line in Fig. 4(a). These results provide support for a conventional phonon-mediated mechanism as the superconducting origin in Li-decorated graphene. For completeness, we also explore the sensitivity of the calculated superconducting energy gap and critical temperature to the choice of the Coulomb parameter μ^* , as shown in Figs. 4(c)-(d). For $\mu^* = 0.12$ and 0.16, we obtain $\Delta_0 = 1.10$ meV and 0.69 meV and

$T_c = 7.6$ and 5.1 K, respectively.

Finally, using the α -model [45, 46], we obtain the temperature dependence of the reduced electronic specific heat in the superconducting state. Within this model, the ratio $\alpha = \Delta_0/k_B T_c$ is an adjustable parameter and the normalized superconducting state electronic entropy S_{es} and heat capacity C_{es} are expressed in terms of $\gamma_n T_c$ as:

$$\frac{S_{es}(t)}{\gamma_n T_c} = -\frac{6\alpha}{\pi^2} \int_0^\infty [f \ln(f) + (1-f) \ln(1-f)] d\tilde{\epsilon}, \quad (7)$$

$$\frac{C_{es}(t)}{\gamma_n T_c} = t \frac{d(S_{es}/\gamma_n T_c)}{dt}, \quad (8)$$

where $f = [\exp(\alpha \tilde{E}/t) + 1]^{-1}$ is the Fermi-Dirac distribution function, $t = T/T_c$ is the reduced temperature, and $\gamma_n = (2/3)\pi^2 k_B^2 N_F$ is the Sommerfeld coefficient. The reduced quasi-particle energy is defined as

$\tilde{E} = \sqrt{\tilde{\varepsilon}^2 + \delta^2(t)}$, where $\tilde{\varepsilon} = \varepsilon/\Delta_0$ is the reduced normal state single-particle energy relative to the Fermi level and $\delta(t) = \Delta(T)/\Delta_0$ is the reduced gap function. The upper limit in the integral in Eq. (7) is set to $500 \gg 1$.

Figure 4(e) shows the calculated $C_{es}/\gamma_n T_c$ for $\alpha = 1.75$. The temperature dependence of the normalized gap $\delta(t)$ is assumed to be the same as in the BCS theory [45, 46]. We checked the numerical results by comparing the data for $\alpha_{BCS} = 1.764$ with Tables II–IV in Ref. [45] and by verifying that the entropy at the critical temperature is equal to that of the normal state. The shape of the calculated specific heat curve is consistent with a one-gap BCS model and undergoes a discontinuous jump at the critical temperature. The specific heat jump at T_c is found to be $\Delta C_e(T_c)/\gamma_n T_c = 1.385$ [shown in the inset of Fig. 4(e)], close to the weak limit BCS value of 1.426 [44]. Furthermore, this result is comparable to the experimental and theoretical values reported for the normalized specific heat jump in bulk CaC_6 [16, 47].

CONCLUSIONS

In conclusion, we have studied the superconducting properties in Li-decorated monolayer graphene within the *ab initio* anisotropic Migdal-Eliashberg theory. Our results provide support for a standard phonon-mediated mechanism at the origin of the superconducting transition. Most of the electron-phonon coupling originates from the low-energy modes dominated by the motion of Li atoms similar to bilayer C_6CaC_6 . We find a sizable anisotropy in the electron-phonon coupling which yields a single anisotropic gap over the Fermi surface. Further enhancement in the critical temperature of LiC_6 is expected in the presence of a substrate [14] or under applied strain [48].

ACKNOWLEDGMENTS

J-J Zheng acknowledges the support from the China Scholarship Council (Grant No. 201508140043).

[1] K. S. Novoselov, V. I. Fal'ko, L. Colombo, P. R. Gellert, M. G. Schwab, and K. Kim, *Nature* **490**, 192 (2012).
 [2] M. Eimenkel and K. B. Efetov, *Phys. Rev. B* **84**, 214508 (2011).
 [3] G. Profeta, M. Calandra, and F. Mauri, *Nat. Phys.* **8**, 131 (2012).
 [4] E. R. Margine and F. Giustino, *Phys. Rev. B* **90**, 014518, (2014).
 [5] B. Uchoa and A. H. Castro Neto, *Phys. Rev. Lett.* **98**, 146801 (2007).
 [6] R. Nandkishore, L. S. Levitov, and A. V. Chubukov, *Nat. Phys.* **8**, 158 (2012).

[7] M. L. Kiesel, C. Platt, W. Hanke, D. A. Abanin, and R. Thomale, *Phys. Rev. B* **86**, 020507(R) (2012).
 [8] B. M. Ludbrook, G. Levy, P. Nigge, M. Zonno, M. Schneider, D. J. Dvorak, C. N. Veenstra, S. Zhdanovich, D. Wong, P. Dosanjh, C. Straßer, A. Stöhr, S. Forti, C. R. Ast, U. Starke, and A. Damascelli, *Proc. Natl. Acad. Sci. USA.* **112**, 11795 (2015).
 [9] S. Ichinokura, K. Sugawara, A. Takayama, T. Takahashi, and S. Hasegawa, *ACS Nano* **10**, 2761 (2016).
 [10] J. Chapman, Y. Su, C. A. Howard, D. Kundys, A. Grigorenko, F. Guinea, A. K. Geim, I. V. Grigorieva, and R. R. Nair, *Sci. Rep.* **6**, 23254 (2016).
 [11] P. B. Allen and B. Mitrović, *Solid State Phys.* **37**, 1 (1982).
 [12] E. R. Margine and F. Giustino, *Phys. Rev. B* **87**, 024505 (2013).
 [13] D. M. Guzman, H. M. Alyahyaei, and R. A. Jishi, *2D Mater.* **1**, 021005 (2014).
 [14] T. P. Kaloni, A. V. Balatsky, and U. Schwingenschlög, *Eur. Phys. Lett.* **104**, 47013 (2013).
 [15] D. Szczyński, A. P. Durajski, and R. Szczyński, *J. Phys.: Condens. Matter* **26**, 255701 (2014).
 [16] A. Sanna, G. Profeta, A. Floris, A. Marini, E. K. U. Gross, and S. Massidda, *Phys. Rev. B* **75**, 020511(R) (2007).
 [17] E. R. Margine, H. Lambert, and F. Giustino, *Sci. Rep.* **6**, 21414 (2016).
 [18] R. Szczyński, E. A. Drzazga, and D. Szczyński, *Eur. Phys. J. B* **88**, 52 (2015).
 [19] D. M. Ceperley and B. J. Alder, *Phys. Rev. Lett.* **45**, 566 (1980).
 [20] J. P. Perdew and A. Zunger, *Phys. Rev. B* **23**, 5048 (1981).
 [21] N. Troullier and J. L. Martins, *Phys. Rev. B* **43**, 1993 (1991).
 [22] M. Fuchs and M. Scheffler, *Comput. Phys. Commun.* **119**, 67 (1999).
 [23] P. Giannozzi *et al.*, *J. Phys. Condens. Matter* **21**, 395502 (2009).
 [24] M. Methfessel and A. T. Paxton, *Phys. Rev. B* **40**, 3616 (1989).
 [25] S. Baroni, S. de Gironcoli, A. Dal Corso, and P. Giannozzi, *Rev. Mod. Phys.* **73**, 515 (2001).
 [26] F. Giustino, M. L. Cohen, and S. G. Louie, *Phys. Rev. B* **76**, 165108 (2007).
 [27] F. Giustino, arXiv:1603.06965.
 [28] J. Noffsinger, F. Giustino, B. D. Malone, C.-H. Park, S. G. Louie, and M. L. Cohen, *Comput. Phys. Commun.* **181**, 2140 (2010).
 [29] S. Poncé, E. R. Margine, C. Verdi, and F. Giustino, *Comput. Phys. Commun.* (2016) doi:10.1016/j.cpc.2016.07.028.
 [30] N. Marzari, A. A. Mostofi, J. R. Yates, I. Souza, and D. Vanderbilt, *Rev. Mod. Phys.* **84**, 1419 (2012).
 [31] A. A. Mostofi, J. R. Yates, Y.-S. Lee, I. Souza, D. Vanderbilt, and N. Marzari, *Comput. Phys. Comm.* **178**, 685 (2008).
 [32] M. Calandra and F. Mauri, *Phys. Rev. Lett.* **95**, 237002 (2005).
 [33] L. Boeri, G. B. Bachelet, M. Giantomassi, and O. K. Andersen, *Phys. Rev. B* **76**, 064510 (2007).
 [34] M. Calandra, A. N. Kolmogorov, and S. Curtarolo, *Phys. Rev. B* **75**, 144506 (2007).
 [35] E. R. Margine and V. H. Crespi, *Phys. Rev. Lett.* **96**,

- 196803 (2006).
- [36] R. Shimizu, K. Sugawara, K. Kanetani, K. Iwaya, T. Sato, T. Takahashi, and T. Hitosugi, *Phys. Rev. Lett.* **114**, 146103 (2015).
- [37] A. V. Fedorov, N. I. Verbitskiy, D. Haberer, C. Struzzi, L. Petaccia, D. Usachov, O. Y. Vilkov, D. V. Vyalikh, J. Fink, M. Knupfer, B. Büchner, and A. Grüneis, *Nat. Commun.* **5**, 3257 (2014).
- [38] J. Kleeman, K. Sugawara, T. Sato, and T. Takahashi, *J. Phys. Soc. Jpn.* **83**, 124715 (2014).
- [39] A. Grüneis, C. Attacalite, A. Rubio, D. V. Vyalikh, S. L. Molodtsov, J. Fink, R. Follath, W. Eberhardt, B. Büchner, and T. Pichler, *Phys. Rev. B* **79** 205106 (2009).
- [40] T. Valla, J. Camacho, Z. H. Pan, A. V. Fedorov, A. C. Walters, C. A. Howard, and M. Ellerby, *Phys. Rev. Lett.* **102**, 107007 (2009).
- [41] S.-L. Yang, J. A. Sobota, C. A. Howard, C. J. Pickard, M. Hashimoto, D. H. Lu, S.-K. Mo, P. S. Kirchmann, and Z.-X. Shen, *Nat. Commun.* **5**, 3493 (2014).
- [42] R. S. Gonnelli, F. Paolucci, E. Piatti, K. Sharda, A. Sola, M. Tortello, J. R. Nair, C. Gerbaldi, M. Bruna, and S. Borini, *Sci. Rep.* **5**, 9554 (2015).
- [43] H. J. Choi, M. L. Cohen, and S. G. Louie, *Physica C* **385**, 66 (2003).
- [44] J. Bardeen, L. N. Cooper, and J. R. Schrieffer, Theory of superconductivity, *Phys. Rev.* **108**, 1175 (1957).
- [45] D. C. Johnston, *Supercond. Sci. Technol.* **26**, 115011 (2013).
- [46] H. Padamsee, J. E. Neighbor, and C. A. Shiffman, *J. Low Temp. Phys.* **12**, 387 (1973).
- [47] J. S. Kim, R. K. Kremer, L. Boeri, and F. S. Razavi, *Phys. Rev. Lett.* **96**, 217002 (2006).
- [48] J. Pešić, R. Gajić, K. Hingerl, and M. Belić, *Europhys. Lett.* **108**, 67005 (2014).